10-18-2019

Scan Parameter Optimization for Histotripsy Treatment of S. Aureus Biofilms on Surgical Mesh

Timothy Bigelow
Iowa State University, bigelow@iastate.edu

Clayton L. Thomas
Iowa State University, clthomas@iastate.edu

Huaiqing Wu
Iowa State University, isuhwu@iastate.edu

Scan Parameter Optimization for Histotripsy Treatment of S. Aureus Biofilms on Surgical Mesh

Abstract

There is a critical need to develop new noninvasive therapies to treat bacteria biofilms. Previous studies have demonstrated the effectiveness of cavitation-based ultrasound histotripsy to destroy these biofilms. In this study, the dependence of biofilm destruction on multiple scan parameters was assessed by conducting exposures at different scan speeds (0.3-1.4 beam widths/sec), step sizes (0.25-0.5 beam widths), and number of passes of the focus across the mesh (2-6). For each of the exposure conditions, the number of colony forming units (CFUs) remaining on the mesh was quantified. A regression analysis was then conducted revealing that scan speed was the most critical parameter for biofilm destruction. Reducing the number of passes and the scan speed should allow for more efficient biofilm destruction in the future reducing the treatment time.

Keywords

Biofilm infection, histotripsy, ultrasound therapy

Disciplines

Biomedical | Cell and Developmental Biology | Electrical and Computer Engineering | Statistics and Probability

Comments

This is a manuscript of an article published as Bigelow, T. A., C. L. Thomas, and H. Wu. "Scan Parameter Optimization for Histotripsy Treatment of S. Aureus Biofilms on Surgical Mesh." *IEEE Transactions on Ultrasonics, Ferroelectrics, and Frequency Control* (2019). DOI: 10.1109/TUFFC.2019.2948305. Posted with permission.

Scan Parameter Optimization for Histotripsy Treatment of *S. Aureus* Biofilms on Surgical Mesh

Timothy A. Bigelow, *Senior Member, IEEE*, Clayton L. Thomas, and Huaiqing Wu

***Abstract*— There is a critical need to develop new noninvasive therapies to treat bacteria biofilms. Previous studies have demonstrated the effectiveness of cavitation-based ultrasound histotripsy to destroy these biofilms. In this study, the dependence of biofilm destruction on multiple scan parameters was assessed by conducting exposures at different scan speeds (0.3-1.4 beam widths/sec), step sizes (0.25-0.5 beam widths), and number of passes of the focus across the mesh (2-6). For each of the exposure conditions, the number of colony forming units (CFUs) remaining on the mesh was quantified. A regression analysis was then conducted revealing that scan speed was the most critical parameter for biofilm destruction. Reducing the number of passes and the scan speed should allow for more efficient biofilm destruction in the future reducing the treatment time.**

***Index Terms*—Biofilm infection, histotripsy, ultrasound therapy**

I. Introduction

THE prevention and treatment of infections on medical implants continues to be a significant challenge in medical care. For example, 95% of urinary tract infections and 87% of bloodstream infections are associated with catheters [1]. The problem is even worse in developing countries where the infection rate can be 2 to 5 times higher depending on the device [2]. In order to treat these infections currently, the implant needs to be removed and a new implant installed due to the formation of bacteria biofilm at the infection site. Bacteria biofilms are structured communities of bacteria encased in a protective matrix that provides protection from antibodies [3, 4] and phagocytes [5, 6]. Bacteria biofilms are also highly resistant to antibiotics [7] due to the reduced growth rate of the bacteria in the biofilm and decreased penetration of antibacterial agents in the biofilm. Destroying the protective matrix of the biofilm would allow antibiotics to treat the bacteria curing the infection without the need for implant removal.

We have already demonstrated the potential of using cavitation-based ultrasound histotripsy to destroy bacteria biofilms noninvasively. *Escherichia coli* (*E. coli*) biofilms grown on glass slides [8] as well as *Pseudomonas aeruginosa* (*P. aeruginosa*) biofilms grown on graphite plates [9] (common material found in heart valves) were both effectively treated by cavitation induced by high-intensity ultrasound exposures. Similar to other histotripsy applications, the high-intensity ultrasound creates a bubble cloud in the tissue that mechanically destroys the adjacent cells [10-16]. Dong et al. have also treated biofilms on catheters at lower ultrasound exposure levels by introducing stabilized microbubbles prior to applying the ultrasound [17]. However, the treatment times were orders of magnitude longer than those needed to disrupt the biofilm using histotripsy based methods.

Given the success of treating the biofilms using cavitation therapies, the next step is to select implants that could most benefit from the proposed new treatment. The treatment of surgical mesh infections following hernia repair are a promising application due to the ease of targeting the lower abdomen with ultrasound as well as the envelopment of the mesh fibers by the cavitation cloud during the ultrasound histotripsy exposures. In addition, mesh infections are some of the most severe complications following hernia repair [18-22]. Mesh infections require removal ~70% of the time with a high risk of hernia re-occurrence following removal of the mesh [18, 22, 23].

Therefore, *Staphylococcus aureus* (*S. aureus*) biofilms were grown on surgical mesh samples and treated with cavitation-based histotripsy exposures [24-26]. *S. aureus* was selected due to its dominance in mesh infections following hernia repair [18, 20, 22]. These studies varied the scan parameters to maximize the destruction of the biofilm while minimizing the risk of damage to adjacent tissue. The studies also demonstrated that the strength of the mesh was not altered by the histotripsy exposures. Also, the best exposures achieved an average reduction in the number of Colony Forming Units (CFUs) of 5.4-$\log_{10}$. As a comparison, a reduction of 6-log10 is how the Food and Drug Administration (FDA) defines high-level disinfection. Many *ex vivo* sterilization methods only achieve a 4-$\log_{10}$ reduction [27-29], and Dong et al. [17] only achieved a 3-$\log_{10}$ reduction in their study. Antibiotics typically result in less than 1-$\log_{10}$ reduction in CFUs for a biofilm [30].

Manuscript received ???; accepted ???. This research was supported by National Institutes of Health (NIH) grant number R21EB020722.

T. A. Bigelow is with the Center for Nondestructive Evaluation, Iowa State University, Ames, IA 50011 (e-mail: bigelow@iastate.edu).

C. L. Thomas was with the Center for Nondestructive Evaluation at the time of the study and is now with the Department of Genetics, Development, and Cell Biology, Iowa State University, Ames, IA 50011 (e-mail: clthomas@iastate.edu).

H. Wu is with the Department of Statistics, Iowa State University, Ames, IA 50011 (e-mail: isuhwu@iastate.edu).

When conducting our prior studies, however, we noticed that the exposure times were relatively long. This could be a problem when translating the therapy to the clinic. Fortunately, cavitation-based histotripsy relies on very low duty cycle pulses at each treatment site. Therefore, multiple treatment sites can be "simultaneously" treated by electronically steering the beam to new locations between treatment pulses when a therapy array is used, dramatically reducing the treatment time [31]. Despite this potential, it is still advantageous to know which parameters should be tuned to minimize the treatment time while maintaining the effectiveness of the therapy.

The goal of this study is to determine the relationship between the scan parameters and the level of biofilm destruction on the mesh. Specifically, we varied the scan speed, step size, and the number of times the focus was scanned over the mesh during the treatment. A regression analysis was then conducted to find a relationship between the scan parameters and the number of surviving CFUs. This relationship could then be used to identify the parameters that could be altered to minimize the treatment time without compromising our effectiveness in treating the biofilms.

II. Methods

A. Biofilm Preparation and Processing

As was done in our previous studies, *Staphylococcus aureus subsp. aureus (ATCC® 25923™)* biofilms were grown on 1 cm x 1 cm Polypropylene mesh samples (PPKM301, Surgical Mesh Division, Textile Development Associates Inc., Brookfield, CT) [24-26]. PPKM301 was selected for the mesh as it is a monofilament mesh with relatively small diameter fibers and large pores. These types of meshes have been shown to have better clinical outcomes when used for hernia repair [19, 32]. To grow robust biofilms, the mesh samples were incubated at 37°C over six days. Growth was initiated by placing the mesh samples in 20 ml of tryptic soy broth (TSB) that had been inoculated with 20 µl of stationary phase bacteria. The following day, and each subsequent day, the samples were transferred to a fresh 20 ml solution of TSB. Fresh TSB was needed each day so that the bacteria would have sufficient nutrients to continue to divide.

After 6 days, the mesh samples were removed from the TSB and inserted into Aquaflex Ultrasound Gel Pad Standoffs (Parker Laboratories Inc., Fairfield, NJ) as was done in our prior studies [24-26]. The gel pad standoffs serve as an easily reproducible sterile tissue mimic for the histotripsy experiments with approximately the same elastic modulus (~53 kPa) as abdominal muscle [33-35]. When assessing cavitation-based tissue damage, it is critical to match the elastic modulus to that of the desired tissue type as the damage to soft tissue is strongly dependent on the modulus [36-42] due to the expansion of the bubble cloud during the histotripsy pulses [39]. While implanted meshes are typically adjacent to both tissue and fluid, having a tissue mimic on both sides would be a reasonable worst-case scenario when assessing the therapy as cavitation would be more suppressed in the tissue relative to the fluid.

To insert the mesh, the gel pads were cut in half. Then, a slit was cut in the middle of the gel pad and the mesh was placed inside of the pad. Then, before allowing the pad to close around the mesh, 100 µl of sterile phosphate buffered saline (PBS) was injected into the slit with the mesh. Any trapped air was then removed by squeezing the gel samples by hand until the air had been released out of the top of the slit. The gel pad was then placed in an aluminum holder that clamped the slit closed. The holder and gel pad/mesh sample were then placed in a room-temperature water tank for the exposure or sham treatments as shown in Fig. 1.

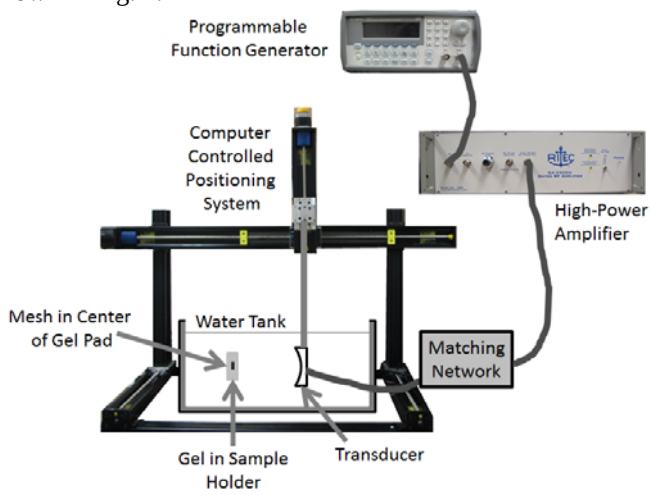

Fig. 1. Experimental setup illustrating the position of the mesh inside of the gel pad during the ultrasound exposures.

Following the exposure or sham treatment, the gel pad with the mesh was removed from the aluminum holder. The edges of the gel pad were then trimmed using a sterile blade leaving only about a 1 cm boarder around the mesh. The gel pad could then be opened and the mesh sample removed due to the slit that had been cut previously when placing the mesh sample in the gel pad. After removal, the mesh sample was briefly dipped in a tube of sterile phosphate buffered saline (PBS) to remove any loose planktonic bacteria. The PBS was free of any contaminants. The mesh was then placed in a 1.5 ml micro-centrifuge tube with 0.5 ml of sterile PBS. The micro-centrifuge tube was subsequently vortexed for one minute, sonicated for two minutes in a Symphony Ultrasonic Cleaner (1.9 L, VWR, Radnor, PA), vortexed for another minute, sonicated for two more minutes, and then vortexed again for one minute. The vortexing disperses the bacteria in the tube while the sonication releases the bacteria from the mesh without killing them. The use of an ultrasonic cleaner to loosen biofilms/bacteria from surfaces is standard practice in microbiology research and does not significantly impact results [43].

After the final vortexing, 0.5 ml was removed from the micro-centrifuge tube and diluted serially in sterile PBS at dilutions of 10^{-1}, 10^{-2}, 10^{-3}, 10^{-4}, and 10^{-5}. Then, 100 µl was removed from each dilution, plated on tryptic soy agar plates, and incubated overnight at 37°C. The number of CFUs on each plate was then counted using established methods [24-26] and used to back calculate the total number of CFUs remaining on

the mesh. The number of CFUs was then translated into a log number for comparison by calculating $\log_{10}$(Number of CFUs+1) for each exposure.

In addition to processing the mesh, the number of CFUs released onto the gel was also determined. For the gel results, the location of the gel pad where the mesh had been placed was scrapped by a sterile blade removing a thin layer of the gel. The gel fragments were then placed in the same tube of PBS where the mesh had been briefly dipped. The PBS tube with the gel fragments was then vortexed for 3 minutes to break up and disperse the fragments. After vortexing, 0.5 ml was removed and diluted serially in sterile PBS at dilutions of 10^{-1}, 10^{-2}, 10^{-3}, 10^{-4}, and 10^{-5}. Following the dilution, 100 µl was once again removed from each dilution, plated on tryptic soy agar plates, and incubated overnight at 37ºC. The number of CFUs released onto the gel was also counted using established methods and translated into a log number. For this study, bacteria released onto the gel only served to confirm the presence of bacteria on the sample. Treating the bacteria in the biofilm on the mesh is the most critical as any released bacteria would be susceptible to the body's natural immune response as well as antibiotics.

B. Ultrasound Exposure Conditions

The ultrasound exposures were conducted using a custom single-element spherically focused transducer (H-184, Sonic Concepts Inc., Bothell, WA). The transducer had a focal length of 63.6 mm and a diameter of 82 mm. The transducer also had a 39.9 mm hole at its center to allow for the placement of an imaging probe to monitor the therapy during future *in vivo* experiments. The transducer was excited by a 3-cycle tone burst at a frequency of 1.3 MHz and a pulse repetition frequency (PRF) of 500 Hz. At this frequency, the 3 dB beam width (BW) of the transducer was 0.7 mm as measured by a wire target. The tone bursts were generated by a programmable function generator (Agilent 33220A, Santa Clara, CA) connected to a high-power pulse amplifier (GA-2500A Gated RF Amplifier, Ritec Inc., Warwick, RI). The signals from the amplifier were fed through a custom matching network prior to reaching the transducer. Backscattered signals were also monitored for cavitation activity and cavitation was observed for all of the exposures except the sham exposures similar to our earlier studies [24-26].

The ultrasound transducer was calibrated by combining modelling and field measurements. Direct field measurements at the focus are often not possible due to the production of inertial cavitation at the tip of the hydrophone potentially damaging the hydrophone. Also, the finite size of the hydrophone will result in a spatial averaging of the higher harmonics introducing errors in the field measurements [44-46]. Therefore, it is best to measure the ultrasound fields away from the focus and then model the waveforms at the focus using numerical methods [47-49]. In this study, the time-domain waveforms were measured in the plane 15 mm in front of the focus using a capsule hydrophone (ONDA HGL-0200, Onda Corporation, Sunnyvale, CA). The measured waveforms were then input into K-Wave (http://www.k-wave.org/index.php) to find the fields throughout the focal region. K-Wave is a free MATLAB tool box that computes nonlinear propagation of ultrasound waves using a generalized form of the Westervelt equation [50].

Similar to our earlier study [26], the K-Wave modelling was broken down into two regions to avoid running out of memory. The first modelling region extended from the measurement plane to 5 mm before the focal plane, extended 36 mm x 36 mm in the lateral dimensions, and supported 20 harmonics. The second modelling region extended from 5 mm in front of the focal plane to 5 mm past the focal plane, extended 13.7 mm x 13.7 mm in the lateral dimensions, and supported 30 harmonics. The lateral dimensions of the second modelling region correspond to when the ultrasound fields had dropped by 20 dB relative to its maximum in the plane 5 mm in front of the focus. The maximum compressional pressure, p_c, was found to be 37 MPa while the maximum rarefactional pressure, p_r, was -10.7 MPa. The calculated waveforms at the locations of peak compressional and rarefactional pressures are shown in Fig. 2. In addition, the peak values of p_c and p_r in the focal region are shown in Fig. 3.

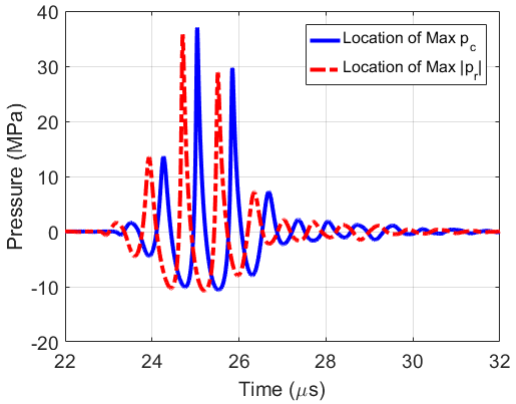

Fig. 2. Waveforms at the location of peak compressional pressure, p_c, and peak rarefactional pressure, p_r, found from the measurement/modelling calibration of the transducer.

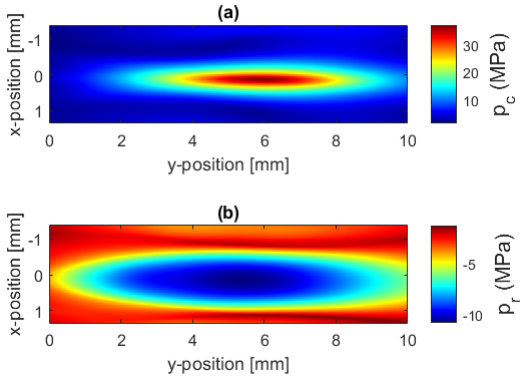

Fig. 3. (a) Peak compression, p_c, and (b) rarefactional, p_r, pressures in the focal region from the measurement/modelling calibration of the transducer.

For the ultrasound exposures, the focus of the transducer was first aligned on the mesh using low-amplitude signals from a pulser-receiver (Panametrics 5900, Olympus Corporation, Tokyo, Japan). Once aligned, the focus was scanned over the entire surface of the mesh with a safety margin of approximately 2 mm on all sides of the mesh. During the scan,

This article has been accepted for publication in a future issue of this journal, but has not been fully edited. Content may change prior to final publication. Citation information: DOI 10.1109/TUFFC.2019.2948305, IEEE Transactions on Ultrasonics, Ferroelectrics, and Frequency Control

Table I: Summary of exposure conditions used in the experiment.

Exposure Condition	Scan Speed, s (BW/sec)	Scan Step Size, δ (BW)	# of Passes, P	# of Repetitions
Sham	NA	NA	Off	79
A	1.4	0.5	2	14
B	1.4	0.25	2	14
C	1.4	0.5	4	9
D	1.4	0.25	4	17
E	1.4	0.5	6	9
F	1.4	0.25	6	9
G	0.7	0.5	2	9
H	0.7	0.5	4	9
I	0.7	0.25	4	9
J	0.7	0.5	6	9
K	0.7	0.25	6	9
L	0.3	0.35	2	9
M	0.3	0.5	4	9
N	0.3	0.35	4	9

the focus was moved continuously in the horizontal direction until the edge of the treatment zone was reached as is illustrated in Fig. 4. Once the edge of the treatment zone was reached, the transducer was stepped in the vertical direction and the continuous scan resumed with the motion now in the opposite direction. Once the scan reached the end of the last row (final focal location), the focus was returned to the initial focal location. The mesh could then be treated by multiple passes of the focus across the surface of the mesh.

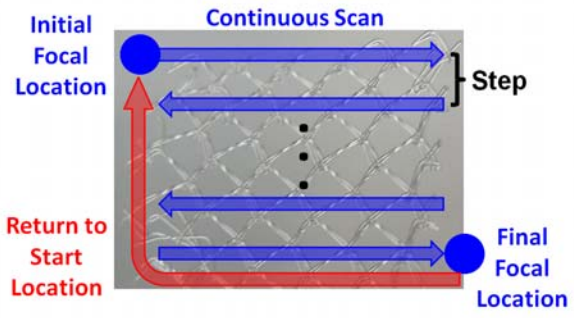

Fig. 4. Illustration of ultrasound exposure parameters where the focal spot was continuously scanned in the horizontal direction, stepped in the vertical direction, and passed over the mesh multiple times when treating the biofilms.

For this study, we varied the scan speed of the continuous portion of the scan, the step between treatment rows, and the number of times the focus was passed over the mesh during an exposure. The scan speeds considered were 0.3, 0.7, and 1.4 BW/sec while the step sizes considered were 0.25, 0.35, and 0.5 BW. These parameters were selected based on exposures that were at least somewhat successful at destroying the biofilm in our earlier studies [25, 26]. The goal of this study was to know how to best modify these parameters in the future to minimize treatment time while maintaining effectiveness. Therefore, we wanted to start with parameters that we already knew were somewhat effective. In addition, the number of times the focus was passed over the mesh was also varied as 2, 4, or 6 passes. The number of passes would be the number of times the treatment was repeated on a single mesh sample. The number of repetitions in Table I is the number of different mesh samples that were treated by the given exposure condition for the purpose of statistical analysis. Conducting experiments with all 27 combinations would have required a very large number of observations. In addition, it would have been impossible to have evaluated the longest exposures given the time required to complete each scan. Therefore, only 14 of the possible combinations were tested. The exact combinations selected were biased towards shorter treatment times as our goal was to reduce the treatment time for future experiments. As a result, the slowest scan speed at the fewest number of cases. The exact cases considered and the number of repetitions for each case are detailed in Table I. In addition, multiple sham exposures were also conducted. For the shams, the infected mesh was also placed in the gel pad in the water tank in an aluminum holder for the same amount of time as the ultrasound exposures. Three of the cases had a larger number of repetitions as the initial treatment results had greater variability than was observed for the other cases. Therefore, additional observations were added to the treatment plan.

After completing the exposures, we analyzed the data using the JMP software (Pro 14, the SAS Institute). We first performed an analysis of variance (ANOVA) that included the scan speed, the step size, and the number of passes as three factors. We then used multiple regression that included the scan speed, the step size, and the number of passes as well as their quadratic terms and interactions. However, the regression analysis predicted a non-physical behavior at higher scan speeds. Specifically, the analysis predicted a decrease in CFUs at scan speeds greater than 1 BW/sec. Upon further examination of the data, the two cases with the highest variance were for the speed of 1.4 BW/sec (i.e., δ = 0.25 BW, P = 4 and δ = 0.5 BW, P = 6). This may have contributed to the non-physical behavior at higher speeds. Given this concern, we restricted our final regression analysis of the data to the speeds of 0.3 and 0.7 BW/sec, with only linear terms of the scan parameters because of a small number of exposure conditions in the data.

This article has been accepted for publication in a future issue of this journal, but has not been fully edited. Content may change prior to final publication. Citation information: DOI 10.1109/TUFFC.2019.2948305, IEEE Transactions on Ultrasonics, Ferroelectrics, and Frequency Control

III. Results

A. Sham Results – Time Dependence

The exposure conditions used in the study spanned a very wide range of treatment times. Therefore, before performing the regression analysis, we needed to confirm that the time the mesh spent in the nutrient-deprived environment of the gel pad did not adversely affect the viability of the bacteria in the biofilm. Fig. 5 and 6 show the numbers of CFUs on the mesh and released onto the gel for the sham exposures as a function of the time the mesh spent in the gel pad. For the range of times relevant for our exposures, time was not a significant factor.

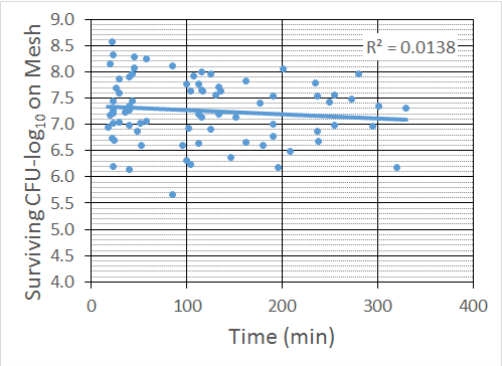

Fig. 5. Count of CFUs surviving on the mesh sample for the sham exposures as a function of treatment time. The R^2 value corresponds to the linear fit shown as the solid line in the graph.

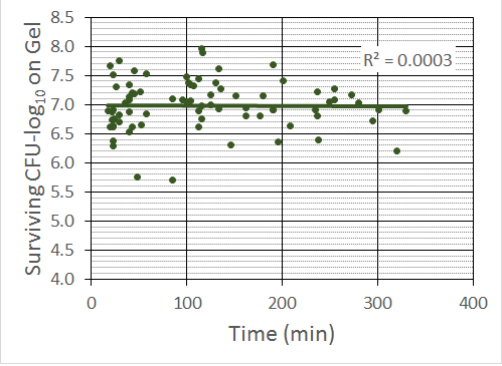

Fig. 6. Count of CFUs surviving on the gel for the sham exposures as a function of treatment time. The R^2 value corresponds to the linear fit shown as the solid line in the graph.

B. Mesh CFU Results

The ANOVA showed that the scan speed, the step size, and the number of passes were all statistically significant (with a p-value of less than 0.01) with the exception of the 0.7 BW/sec scan speed (average of 3.79-$\log_{10}$ CFUs) and the 1.4 BW/sec scan speed (average of 3.83-$\log_{10}$ CFUs) which were not statistically significantly different. Hence, as discussed at the end of Section II, we restricted our final regression analysis to scan speeds of 0.3 and 0.7 BW/sec. Recall, that our goal is to use the analysis to predict exposure conditions that could effectively treat bacteria biofilms in the future without needing to explore the entire sample space. Since the scan speed of 1.4 BW/sec never gave us the desired level of biofilm destruction, there was little reason to focus on this region of the parameter space in this study.

After the regression, the number of CFUs remaining on the mesh was predicted to be given by

$$N_{CFU} = \begin{bmatrix} 0.255 + 4.818 \cdot s \\ +4.711 \cdot \delta - 0.383 \cdot P \end{bmatrix} \quad (1)$$

where N_{CFU} is the number of CFUs in $\log_{10}$, s is the scan speed in BW/sec, P is the number of passes the focus made across the mesh for each exposure, and δ is the step size in BW. Fig. 7 shows the number of CFUs remaining on the mesh for each of the exposure conditions considered in the study along with the prediction from (1). The average number of CFUs on the mesh for the sham exposures is also included for a comparison as are the results for the 1.4 BW/sec exposures even though these values were not included in the final regression analysis. There is reasonably good agreement between the regression analysis-predicted values and the measured values for scan speeds of 0.3 and 0.7 BW/sec where the fit was performed. The lack-of-fit test shows that there is no lack of fit with this statistical fit (p-value of 0.10, F-ratio of 2.04). The root mean square error (RMSE) for the fit is 1.31. The lack of a change in measured CFUs between the 1.4 BW/sec exposures (average of 3.79-$\log_{10}$ CFUs) and 0.7 BW/sec exposures (average of 3.83-$\log_{10}$ CFUs) is also evident from the figure.

Fig. 8, 9, and 10 show the predicted numbers of CFUs remaining on the mesh for step sizes between 0.25 and 0.5 BW, scan speeds between 0.3 and 0.7 BW/sec, and the number of passes between 2 and 6. The two surfaces in each plot correspond to the maximum and minimum values of the variable that is not shown on the x or y axis. Hence, for Fig. 8, the two surfaces correspond to step sizes of 0.25 and 0.5 BW; for Fig. 9, the surfaces correspond to 2 and 6 passes; and for Fig. 10, the surfaces correspond to scan speeds of 0.3 and 0.7 BW/sec. From these figures, it is clear that the scan speed has the greatest impact on the number of CFUs.

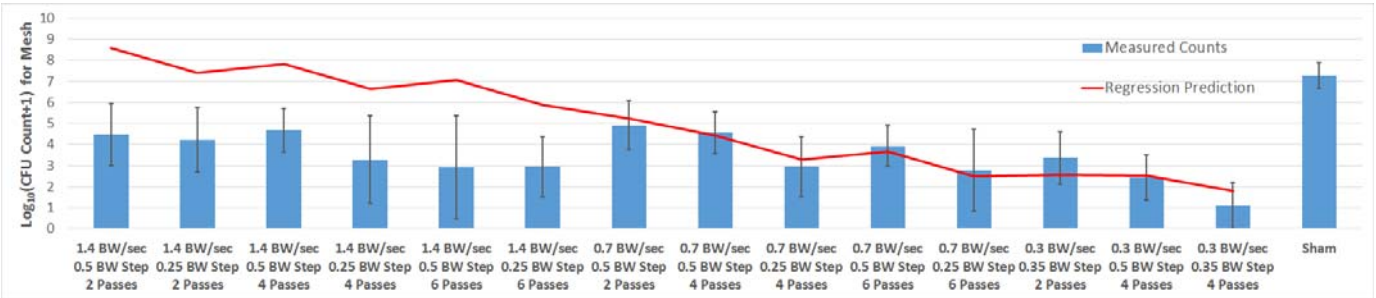

Fig. 7. Count of CFUs surviving on the mesh sample following the treatment for all of the exposure conditions considered in the study (bars) along with the predicted values based on the regression analysis (line). The error bars correspond to one standard deviation for the measured values.

This article has been accepted for publication in a future issue of this journal, but has not been fully edited. Content may change prior to final publication. Citation information: DOI 10.1109/TUFFC.2019.2948305, IEEE Transactions on Ultrasonics, Ferroelectrics, and Frequency Control

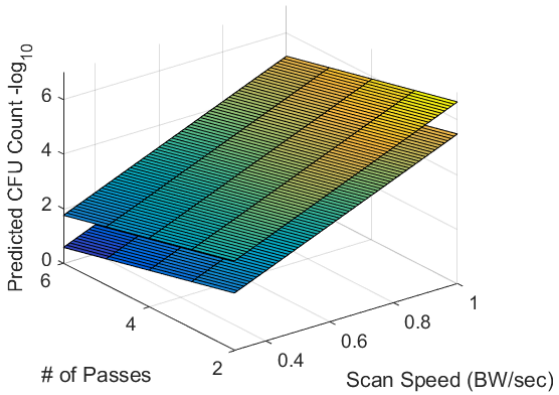

Fig. 8. Predicted number of CFUs surviving on the mesh as a function of the scan speed and the number of passes for step sizes of 0.25 BW (lower surface) and 0.5 BW (upper surface).

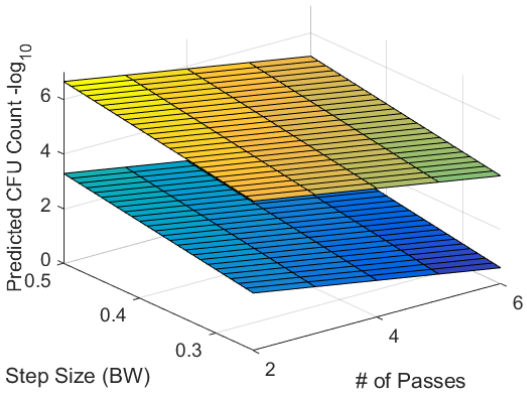

Fig. 10. Predicted number of CFUs surviving on the mesh as a function of the step size and the number of passes for scan speeds of 0.3 BW/sec (lower surface) and 0.7 BW/sec (upper surface).

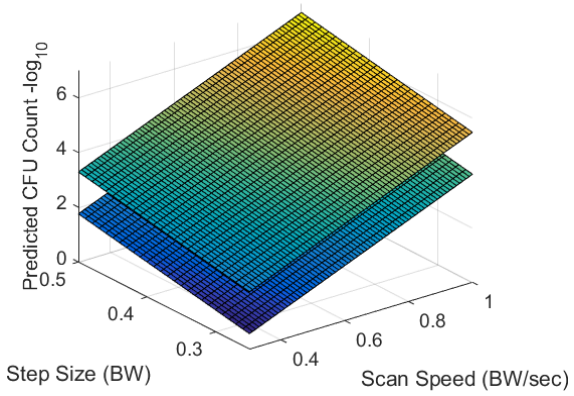

Fig. 9. Predicted number of CFUs surviving on the mesh as a function of the scan speed and the step size for numbers of passes of 6 (lower surface) and 2 (upper surface).

Decreasing the scan speed results in a relatively rapid reduction in the number of CFUs. The dependence on the number of passes is also significant, but it is not as pronounced as the dependence on the scan speed. The variation in N_{CFU} with the step size is the least significant over the range of step sizes considered in this study. While not assessed, it is likely that increasing the step size much beyond 0.5 BW would result in portions of the mesh sample not being treated by the bubble cloud.

IV. Discussion

The lack of statistical difference between the 0.7 BW/sec and 1.4 BW/sec scan speeds was surprising. It would seem that the level of biofilm destruction should monotonically increase as the scan speed is reduced. The lack of a decrease in CFUs between 1.4 BW/sec and 0.7 BW/sec may suggest a plateau in the exposure conditions where it is easy to reduce the number of CFUs by 3 to 4-log10 for modest exposures over a wide range. Perhaps these bacteria are not as tightly adhered to the biofilm and easier to strip away. However, longer exposures to cavitation are needed to destroy the heart of the biofilm. It may be that a similar plateau could be found for the other exposure parameters should they also be varied over a wider range. It may be useful to explore the higher-speed parameter space in more detail in the future so that the physics of the biofilm destruction by cavitation can be better understood.

After performing the linear regression analysis, the study demonstrated that the scan speed has the greatest impact on the number of CFUs surviving on the mesh samples following the ultrasound treatment. The regression analysis yielded the approximate relationship between the scan parameters and the number of surviving CFUs. One way to assess the robustness of the analysis is to compare the regression analysis-predicted values to the results from our prior studies. However, since the growth conditions were different for some of our prior studies, it is best to compare the reduction in CFUs relative to the sham rather than the number of CFUs remaining on the mesh. Since

Table II: Comparison of predicted values to results from prior studies.

Reference to Published Study	[25]	[25]	[25]	[25]	[26]
Scan Speed, *s* (BW/sec)	1 BW/sec	1.33 BW/sec	0.67 BW/sec	0.67 BW/sec	0.23 BW/sec
Scan Step Size, δ (BW)	0.3 BW	0.3 BW	0.6 BW	0.3 BW	0.3 BW
# of Passes, *P*	5	5	5	5	4
Measured Beam Width (mm)	1.2 mm	1.2 mm	1.2 mm	1.2 mm	1.3 mm
Focal Length of Transducer (mm)	125 mm	125 mm	125 mm	125 mm	63.6 mm
PRF (Hz)	1000 Hz	1000 Hz	1000 Hz	1000 Hz	500 Hz
Frequency (MHz)	1.1 MHz	1.1 MHz	1.1 MHz	1.1 MHz	0.9 MHz
Number of Cycles in Pulse	10	10	10	3	3
Measured Reduction in CFU-log$_{10}$	3.8±0.8-log$_{10}$	3.8±0.9-log$_{10}$	3.2±1.4-log$_{10}$	3.7±1.2-log$_{10}$	5.4±1.7-log$_{10}$
Predicted Reduction in CFU-log$_{10}$	2.7-log$_{10}$	1.1-log$_{10}$	2.9-log$_{10}$	4.3-log$_{10}$	6.1-log$_{10}$
% Difference	-39%	-233%	-10.1%	14.3%	10.7%

the number of CFUs on the meshes in our sham exposures was 7.3±0.6-$\log_{10}$, the expression in (1) can be rewritten to predict the reduction in CFUs as

$$R_{CFU} = \begin{bmatrix} 7.045 - 4.818 \cdot s \\ -4.711 \cdot \delta + 0.383 \cdot P \end{bmatrix} \quad (2)$$

where R_{CFU} is the predicted reduction in CFUs relative to the sham exposures. Table II gives the scan parameters and reduction in CFUs from our prior studies [25, 26], the reduction in CFUs predicted from (2), and the percent difference from the measured and predicted values. To avoid biasing our results, we only included the cases for which at least two of the mesh samples had some surviving CFUs for a given exposure condition. It is not possible to get an accurate measurement of CFU reduction for comparison when no bacteria are left to count.

The regression analysis did not include the data from these prior studies, so the agreement is surprisingly good with errors on the order of 10% to 15% for most exposures. The largest difference is for the 1 BW/sec and 1.33 BW/sec scan speed from [25]. However, this is outside of the range of our regression analysis. In addition, the plateau mentioned previously is also evident in this data. Namely, the 1 BW/sec and 1.33 BW/sec scan speeds have the same measured reduction in CFUs. Hence, including this plateau in the regression analysis would likely lead to better prediction results. However, in order to include this plateau properly, more experiments would need to be conducted in this scan speed range.

Since the agreement between our prior studies and our current regression analysis is reasonable, (2) should be reasonable when selecting scan parameters to evaluate in the future for scan speeds of 0.7 BW/sec or less. Also, there does not seem to be a strong dependence on the number of cycles in the pulse or the PRF. The lack of dependence on the number of cycles in the pulse is in agreement with our prior work [24, 25], and is promising as the collateral tissue damage tends to increase as the duration of the pulse increases [24, 38, 51, 52].

The lack of a dependence on the PRF is also to be expected over the range of PRFs considered as the bubble cloud generated by the histotripsy pulses would not have time to dissipate before the arrival of the next pulse for any of the exposures tested. This phenomenon has been studied in detail by other researchers and is known as cavitation memory [31, 53-56]. In the future, we should be able to reduce the treatment time and improve the efficiency of the treatment by including lower amplitude pulses between the histotripsy pulses to coalesce the bubbles reducing the impact of cavitation memory [55, 56]. The removal of cavitation memory will likely have an impact on the regression analysis provided in this section and may allow for faster scan speeds to be more effective during the treatment. Therefore, additional regression analysis should be conducted as we continue to refine the treatment.

With the robustness of the regression analysis established, we can use it to predict which exposure conditions would allow for faster treatment times while maintaining a reasonable level of biofilm destruction. Fig. 11 shows a normalized scan time estimate as a function of the number of passes, P, and the scan speed, s, for a range of exposures that resulted in at least a 5-$\log_{10}$ reduction in CFUs. The normalized time was found from

$$Normalized \quad Time = \frac{\left(\frac{P}{s \cdot \delta}\right)}{\max\left(\frac{P}{s \cdot \delta}\right)} \quad (3)$$

The figure also includes the experimental results from the present study as well as our previous study [26] which achieved at least a 5-$\log_{10}$ reduction in CFUs. In order to provide additional guidance, we extended the scan speed range from 0.3-0.7 BW/sec to 0.2-0.7 BW/sec. Therefore, we are extrapolating the results of our regression analysis outside the original range. Extrapolation following regression analysis can lead to errors [57]; however, our experimental results from [26] for a scan speed of 0.23 BW/sec was in agreement with our regression analysis. Therefore, the extrapolation over this narrow range is likely reasonable in this case. From this figure, it is clear that operating at a lower scan speeds with a smaller number of passes should reduce the treatment time by at least a factor of 2 relative to our prior results while maintaining reasonable biofilm destruction. This would translate to treatment times on the order of 12 min/cm^2 in the absences of electronic steering. In the future, additional test cases should be evaluated in this range to further improve the speed of the treatments. Specifically, we should consider single-pass treatments with scan speeds in the range of 0.2 to 0.3 BW/sec.

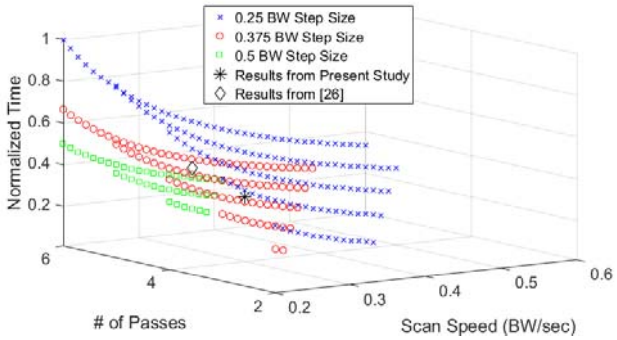

Fig. 11. Estimate of normalized time as a function of scan speed and the number of passes for three different step sizes.

A treatment time of 12 min/cm^2 is still relatively slow for clinical applications given that hernia meshes are typically on the order of 100 cm^2. Therefore, electronic steering will be needed in the future to make the treatment practical as was described previously [31]. Specifically, histotripsy pulses operate at very low duty cycles. When using a single-element transducer, the transducer must be off between the pulses. However, an array can steer every pulse to a different location allowing the transducer elements to be active a greater percentage of the time even though the pulses are going to different locations on the mesh. Therefore, while the beam is being "scanned" in one direction at a rate of 0.2 to 0.3 BW/sec, pulses can be sent to 50 to 100 of other locations on the mesh before returning to the original scan line. Given that we found slow scan speeds to be optimal, a combination of mechanical and electronic focal steering will likely result in the optimal

treatment parameters. Utilizing electronic steering will likely reduce the treatment times by at least a factor of 50, reducing the overall treatment times from over 20 hours to less than 30 minutes.

V. CONCLUSION

In this study, we explored the impact of the scan speed, the step size, and the number of passes on biofilm destruction on hernia mesh samples. A regression analysis was then conducted to guide future parameter selection to minimize exposure time. The scan speed had the largest impact on biofilm destruction. Reducing the scan speed and the number of passes should result in more efficient biofilm destruction. Reducing the treatment time is critical if the therapy is to be translated to the clinic.

REFERENCES

[1] M. J. Richards, J. R. Edwards, D. H. Culver, and R. P. Gaynes, "Nosocomial infections in medical intensive care units in the United States," *Critical Care Medicine,* vol. 27, pp. 887-892, 1999.

[2] V. D. Rosenthal, H. Bijie, D. G. Maki, Y. Mehta, A. Apisarnthanarak, E. A. Medeiros, *et al.*, "International Nosocomial Infection Control Consortium (INICC) report, data summary of 36 countries, for 2004-2009," *American Journal of Infection Control,* vol. 40, pp. 396-407, 2012.

[3] D. M. Cochrane, M. R. Brown, H. Anwar, P. H. Weller, K. Lam, and J. W. Costerton, "Antibody response to *Pseudomonas aeruginosa* surface protein antigens in a rat model of chronic lung infection," *Journal of Medical Microbiology,* vol. 27, pp. 255-261, 1988.

[4] D. De Beer, P. Stoodley, and Z. Lewandowski, "Measurement of local diffusion coefficients in biofilms by microinjection and confocal microscopy," *Biotechnology and Bioengineering,* vol. 53, pp. 151-158, 1997.

[5] J. Rodgers, F. Phillips, and C. Olliff, "The effects of extracellular slime from *Staphylococcus epidermidis* on phagocytic ingestion and killing," *FEMS Immunology and Medical Microbiology,* vol. 9, pp. 109-115, 1994.

[6] C. Vuong, J. M. Voyich, E. R. Fischer, K. R. Braughton, A. R. Whitney, F. R. DeLeo, *et al.*, "Polysaccharide intercellular adhesin (PIA) protects *Staphylococcus epidermidis* against major components of the human innate immune system," *Cellular Microbiology,* vol. 6, pp. 269-275, 2004.

[7] M. E. Olson, H. Ceri, D. W. Morck, A. G. Buret, and R. R. Read, "Biofilm bacteria: formation and comparative susceptibility to antibiotics," *Canadian Journal of Veterinary Research,* vol. 66, pp. 86-92, 2002.

[8] T. A. Bigelow, T. Northagen, T. M. Hill, and F. C. Sailer, "The destruction of *Escherichia coli* biofilms using high-intensity focused ultrasound," *Ultrasound in Medicine & Biology,* vol. 35, pp. 1026-1031, 2009.

[9] J. Xu, T. A. Bigelow, L. J. Halverson, J. M. Middendorf, and B. Rusk, "Minimization of treatment time for *in vitro* 1.1 MHz destruction of *Pseudomonas aeruginosa* biofilms by high-intensity focused ultrasound," *Ultrasonics,* vol. 52, pp. 668-675, 2012.

[10] Z. Xu, J. B. Fowlkes, A. Ludomirsky, and C. A. Cain, "Investigation of intensity thresholds for ultrasound tissue erosion," *Ultrasound in Medicine & Biology,* vol. 31, pp. 1673-1682, 2005.

[11] Z. Xu, J. B. Fowlkes, E. D. Rothman, A. M. Levin, and C. A. Cain, "Controlled ultrasound tissue erosion: The role of dynamic interaction between insonation and microbubble activity," *The Journal of the Acoustical Society of America,* vol. 117, pp. 424-435, 2005.

[12] Z. Xu, A. Ludomirsky, L. Y. Eun, T. L. Hall, B. C. Tran, J. B. Fowlkes, *et al.*, "Controlled ultrasound tissue erosion," *IEEE Transactions on Ultrasonics, Ferroelectrics, and Frequency Control,* vol. 51, pp. 726-736, 2004.

[13] Z. Xu, J. B. Fowlkes, and C. A. Cain, "A new strategy to enhance cavitational tissue erosion using a high-intensity, initiating sequence," *IEEE Transactions on Ultrasonics, Ferroelectrics, and Frequency Control,* vol. 53, pp. 1412-1424, 2006.

[14] W. W. Roberts, "Focused ultrasound ablation of renal and prostate cancer: Current technology and future directions," *Urologic Oncology: Seminars and Original Investigations,* vol. 23, pp. 367-371, 2005.

[15] T. L. Hall, J. B. Fowlkes, and C. A. Cain, "Imaging feedback of tissue liquefaction (histotripsy) in ultrasound surgery," in *2005 IEEE Ultrasonics Symposium,* pp. 1732-1734, 2005.

[16] J. E. Parsons, C. A. Cain, G. D. Abrams, and J. B. Fowlkes, "Pulsed cavitational ultrasound therapy for controlled tissue homogenization," *Ultrasound in Medicine & Biology,* vol. 32, pp. 115-129, 2006.

[17] Y. Dong, J. Li, P. Li, and J. Yu, "Ultrasound microbubbles enhance the activity of Vancomycin against *Staphylococcus epidermidis* biofilms *in vivo*," *Journal of Ultrasound in Medicine,* vol. 37, pp. 1379-1387, 2018.

[18] M. Mavros, S. Athanasiou, V. Alexiou, P. Mitsikostas, G. Pepp as, and M. Falagas, "Risk factors for mesh-related infections after hernia repair surgery: A meta-analysis of cohort studies," *World Journal of Surgery,* vol. 35, pp. 2389-2398, 2011.

[19] P. Amid, "Classification of biomaterials and their related complications in abdominal wall hernia surgery," *Hernia,* vol. 1, pp. 15-21, 1997.

[20] M. E. Falagas and S. K. Kasiakou, "Mesh-related infections after hernia repair surgery," *Clinical Microbiology and Infection,* vol. 11, pp. 3-8, 2005.

[21] T. Lüning and E. J. Spillenaar-Bilgen, "Parastomal hernia: complications of extra-peritoneal onlay mesh placement," *Hernia,* vol. 13, pp. 487-490, 2009.

[22] V. M. Sanchez, Y. E. Abi-Haidar, and K. M. F. Itani, "Mesh infection in ventral incisional hernia repair: Incidence, contributing factors, and treatment," *Surgical Infections,* vol. 12, pp. 205-210, 2011.

[23] K. A. LeBlanc, "Laparoscopic incisional and ventral hernia repair: Complications—how to avoid and handle," *Hernia,* vol. 8, pp. 323-331, 2004.

[24] T. A. Bigelow, C. L. Thomas, H. Wu, and K. M. F. Itani, "Histotripsy treatment of *S. aureus* biofilms on surgical mesh samples under varying pulse durations," *IEEE Transactions on Ultrasonics, Ferroelectrics, and Frequency Control,* vol. 64, pp. 1420-1428, 2017.

[25] T. A. Bigelow, C. L. Thomas, H. Wu, and K. M. F. Itani, "Histotripsy treatment of *S. Aureus* biofilms on surgical mesh samples under varying scan parameters," *IEEE Transactions on Ultrasonics, Ferroelectrics, and Frequency Control,* vol. 65, pp. 1017-1024, 2018.

[26] T. A. Bigelow, C. L. Thomas, H. Wu, and K. M. F. Itani, "Impact of high-intensity ultrasound on strength of surgical mesh when treating biofilm infections," *IEEE Transactions on Ultrasonics, Ferroelectrics, and Frequency Control,* vol. 66, pp. 38-44, 2019.

[27] W. A. Rutala and D. J. Weber, "Reprocessing endoscopes: United States perspective," *Journal of Hospital Infection,* vol. 56, pp. 27-39, 2004.

[28] W. A. Rutala and D. J. Weber, "FDA labeling requirements for disinfection of endoscopes: A counterpoint," *Infection Control and Hospital Epidemiology,* vol. 16, pp. 231-235, 1995.

[29] Q. Liu, M. Zhang, Z. Fang, and X. Rong, "Effects of ZnO nanoparticles and microwave heating on the sterilization and product quality of vacuum-packaged Caixin," *Journal of the Science of Food and Agriculture,* pp. 2547-2554, 2014.

[30] J. N. Anderl, M. J. Franklin, and P. S. Stewart, "Role of antibiotic penetration limitation in *Klebsiella pneumoniae* biofilm resistance to Ampicillin and Ciprofloxacin," *Antimicrobial Agents and Chemotherapy,* vol. 44, p. 1818, 2000.

[31] J. E. Lundt, S. P. Allen, J. Shi, T. L. Hall, C. A. Cain, and Z. Xu, "Non-invasive, rapid ablation of tissue volume using histotripsy," *Ultrasound in Medicine & Biology,* vol. 43, pp. 2834-2847, 2017.

[32] B. Klosterhalfen and U. Klinge, "Retrieval study at 623 human mesh explants made of polypropylene—impact of mesh class and indication for mesh removal on tissue reaction," *Journal of Biomedical Materials Research Part B: Applied Biomaterials,* pp. 1393-1399, 2013.

[33] S. H. M. Brown, J. A. Carr, S. R. Ward, and R. L. Lieber, "Passive mechanical properties of rat abdominal wall muscles suggest an

important role of the extracellular connective tissue matrix," *Journal of Orthopaedic Research,* vol. 30, pp. 1321-1326, 2012.

[34] I. V. Ogneva, D. V. Lebedev, and B. S. Shenkman, "Transversal stiffness and Young's modulus of single fibers from rat soleus muscle probed by atomic force microscopy," *Biophysical Journal,* vol. 98, pp. 418-424, 2010.

[35] F. Dogan and M. S. Celebi, "Quasi-non-linear deformation modeling of a human liver based on artificial and experimental data," *The International Journal of Medical Robotics and Computer Assisted Surgery,* vol. 12, pp. 410-420, 2016.

[36] J. Xu and T. A. Bigelow, "Experimental investigation of the effect of stiffness, exposure time and scan direction on the dimension of ultrasound histotripsy lesions," *Ultrasound in Medicine & Biology,* vol. 37, pp. 1865-1873, 2011.

[37] J. Xu, T. A. Bigelow, G. Davis, A. Avendano, P. Shrotriya, K. Bergler, *et al.*, "Dependence of ablative ability of high-intensity focused ultrasound cavitation-based histotripsy on mechanical properties of agar," *The Journal of the Acoustical Society of America,* vol. 136, pp. 3018-3027, 2014.

[38] J. Xu, T. A. Bigelow, and R. Nagaraju, "Precision control of lesions by high-intensity focused ultrasound cavitation-based histotripsy through varying pulse duration," *IEEE Transactions on Ultrasonics, Ferroelectrics, and Frequency Control,* vol. 60, pp. 1401-1411, 2013.

[39] E. Vlaisavljevich, Y. Kim, G. Owens, W. Roberts, C. Cain, and Z. Xu, "Effects of tissue mechanical properties on susceptibility to histotripsy-induced tissue damage," *Physics in Medicine and Biology,* vol. 59, pp. 253-270, 2014.

[40] E. Vlaisavljevich, K.-W. Lin, A. Maxwell, M. T. Warnez, L. Mancia, R. Singh, *et al.*, "Effects of ultrasound frequency and tissue stiffness on the histotripsy intrinsic threshold for cavitation," *Ultrasound in Medicine & Biology,* vol. 41, pp. 1651-1667, 2015.

[41] E. Vlaisavljevich, A. Maxwell, M. Warnez, E. Johnsen, C. Cain, and X. Zhen, "Histotripsy-induced cavitation cloud initiation thresholds in tissues of different mechanical properties," *IEEE Transactions on Ultrasonics, Ferroelectrics, and Frequency Control* vol. 61, pp. 341-352, 2014.

[42] K. B. Bader, "The influence of medium elasticity on the prediction of histotripsy-induced bubble expansion and erythrocyte viability," *Physics in Medicine & Biology,* vol. 63, p. 095010, 2018.

[43] E. Joyce, T. J. Mason, S. S. Phull, and J. P. Lorimer, "The development and evaluation of electrolysis in conjunction with power ultrasound for the disinfection of bacterial suspensions," *Ultrasonics Sonochemistry,* vol. 10, pp. 231-234, 2003.

[44] Y. Liu, K. A. Wear, and G. R. Harris, "Variation of high-intensity therapeutic ultrasound (HITU) pressure field characterization: Effects of hydrophone choice, nonlinearity, spatial averaging and complex deconvolution," *Ultrasound in Medicine & Biology,* vol. 43, pp. 2329-2342, 2017.

[45] E. G. Radulescu, P. A. Lewin, A. Goldstein, and A. Nowicki, "Hydrophone spatial averaging corrections from 1 to 40 MHz," *IEEE Transactions on Ultrasonics, Ferroelectrics, and Frequency Control,* vol. 48, pp. 1575-1580, 2001.

[46] G. Xing, P. Yang, L. He, and X. Feng, "Spatial averaging effects of hydrophone on field characterization of planar transducer using Fresnel approximation," *Ultrasonics,* vol. 71, pp. 51-58, 2016.

[47] M. S. Canney, M. R. Bailey, and L. A. Crum, "Acoustic characterization of high intensity focused ultrasound fields: A combined measurement and modeling approach," *The Journal of the. Acoustical Society of America,* vol. 124, pp. 2406-2420, 2008.

[48] O. A. Sapozhnikov, S. A. Tsysar, V. A. Khokhlova, and W. Kreider, "Acoustic holography as a metrological tool for characterizing medical ultrasound sources and fields," *The Journal of the Acoustical Society of America,* vol. 138, pp. 1515-1532, 2015.

[49] P. V. Yuldashev, W. Kreider, O. A. Sapozhnikov, N. Farr, A. Partanen, M. R. Bailey, *et al.*, "Characterization of nonlinear ultrasound fields of 2D therapeutic arrays," *IEEE International Ultrasonics Symposium,* vol. 2012, pp. 1-4, 2012.

[50] B. E. Treeby, J. Jaros, A. P. Rendell, and B. T. Cox, "Modeling nonlinear ultrasound propagation in heterogeneous media with power law absorption using a k-space pseudospectral method," *The Journal of the Acoustical Society of America,* vol. 131, pp. 4324-4336, 2012.

[51] Z. Xi, G. E. Owens, H. S. Gurm, D. Yu, C. A. Cain, and X. Zhen, "Noninvasive thrombolysis using histotripsy beyond the intrinsic threshold (microtripsy)," *IEEE Transactions on Ultrasonics, Ferroelectrics, and Frequency Control,* vol. 62, pp. 1342-1355, 2015.

[52] K. W. Lin, Y. Kim, A. D. Maxwell, T. Y. Wang, T. L. Hall, Z. Xu, *et al.*, "Histotripsy beyond the intrinsic cavitation threshold using very short ultrasound pulses: microtripsy," *IEEE Transactions on Ultrasonics, Ferroelectrics, and Frequency Control,* vol. 61, pp. 251-265, 2014.

[53] T.-Y. Wang, Z. Xu, T. L. Hall, J. B. Fowlkes, and C. A. Cain, "An efficient treatment strategy for histotripsy by removing cavitation memory," *Ultrasound in Medicine & Biology,* vol. 38, pp. 753-766, 2012.

[54] A. P. Duryea, C. A. Cain, W. W. Roberts, T. L. Hall, A. P. Duryea, C. A. Cain, *et al.*, "Removal of residual cavitation nuclei to enhance histotripsy fractionation of soft tissue," *IEEE Transactions on Ultrasonics, Ferroelectrics, and Frequency Control,* vol. 62, pp. 2068-2078, 2015.

[55] A. Shi, J. Lundt, Z. Deng, J. Macoskey, H. Gurm, G. Owens, *et al.*, "Integrated histotripsy and bubble coalescence transducer for thrombolysis," *Ultrasound in Medicine & Biology,* vol. 44, pp. 2697-2709, 2018.

[56] A. Shi, Z. Xu, J. Lundt, H. A. Tamaddoni, T. Worlikar, and T. L. Hall, "Integrated histotripsy and bubble coalescence transducer for rapid tissue ablation," *IEEE Transactions on Ultrasonics, Ferroelectrics, and Frequency Control,* vol. 65, pp. 1822-1831, 2018.

[57] G. J. Hahn, "The hazards of extrapolation in regression analysis," *Journal of Quality Technology,* vol. 9, pp. 159-165, 1977.